

pubs.acs.org/JPCC Article

Increasing Photoinduced Interfacial Charge Separation Lifetime through Control of the Twist Angle in the Donor Region of Carbazole-Based Dyes

Christine Curiac, Ethan C. Lambert, Leigh Anna Hunt, Mallory Roberts, Ainsley LaMore, Adithya Peddapuram, Hammad Cheema, Nathan I. Hammer, and Jared H. Delcamp*



Cite This: https://doi.org/10.1021/acs.jpcc.3c04735



ACCESS I

III Metrics & More

Article Recommendations

Supporting Information

ABSTRACT: Molecular-based optoelectronic devices and photocatalytic systems often rely on the photogeneration of charge-separated states. Increasing the longevity of charge-separated states allows for access to higher-functioning devices and systems by extending the length of time before subsequent events are required to occur. In dye-sensitized solar cells (DSC), back electron transfer (BET) from a reduced metal oxide to an oxidized dye is an unproductive electron transfer pathway that determines the charge-separated state lifetime. This study seeks to limit BET by lowering the electronic coupling of the donor and acceptor in the charge-separated excited state through the use of sterics. A series of three dyes with a varying number of methyl groups (0–2) on the donor were studied using nanosecond transient absorption spectroscopy (nsTAS) to compare rates of BET. Novel dye CC10 (1 Me), designed with one methyl group in the

R=H, H \rightarrow R=CH₃, H

22x slower back electron transfer

donor region connected to the acceptor, was found to lower back electron transfer rates by 22× compared to the control dye, CC12 (0 Me), with no methyl groups.

1. INTRODUCTION

Photoinduced electron transfer reactions are vital in a variety of applications in energy conversion fields and in catalysis. Photovoltaics such as dye-sensitized solar cells (DSCs) work through a series of charge transfers after photon absorption to convert light to electricity. DSCs are of current interest due to the high yield of light-to-electricity conversion (particularly in indoor lighting) and are also known to be cost-effective and tunable to the irradiation source and have a relative ease of fabrication. 1-8 DSCs operate via three electron transfer reactions—(1) injection, (2) collection, and (3) regeneration—as described in the following sentences. Photoexcitation of a surface-bound chromophore begins the electron transfer reactions by enabling the injection of an electron into the conduction band (CB) of a semiconductor (typically TiO_2) (step 1, injection). The electron then travels across an external circuit to a counter electrode (typically platinum) before being collected by an oxidized redox shuttle (step 2, collection). The reduced redox shuttle then completes the circuit by regenerating the neutral state of the chromophore (step 3, regeneration). However, unbeneficial electron transfer reactions are possible as well. The electron transfer reaction from reduced TiO2 to an oxidized chromophore is known as back electron transfer (BET). The rate of BET can compete with beneficial electron transfers (collection and regeneration),

thereby reducing DSC device performance. Therefore, limiting the rate of BET is desirable to favor productive pathways.

Several studies have focused on slowing down the rate of BET^{4,9–14} in DSC devices with example studies focused on controlling dye structure, ^{9,13,14} adding semiconductor surface insulators, ^{8,10,12} adjusting surface charge, ¹¹ and controlling dye-redox shuttle preorganization. ¹² Slowing BET has been shown to improve the open-circuit voltage ($V_{\rm oc}$) and fill factor (FF), among other parameters. ^{12,15} A variety of designs related to the dye structure have been utilized in the literature to slow BET. Figure 1 compares methods of slowing BET among two select literature examples and this work. The first example study probed the effect of increasing the distance between the donor and the acceptor regions of the dye molecule, portrayed through dyes **Star YZ1** and **Star YZ2**. ¹⁶ The rate of BET decreased by about 6× when comparing **Star YZ2** to **Star YZ1**. Although this approach significantly slowed the back electron transfer reaction, it simultaneously slowed the excited-state

Received: July 13, 2023 Revised: September 28, 2023



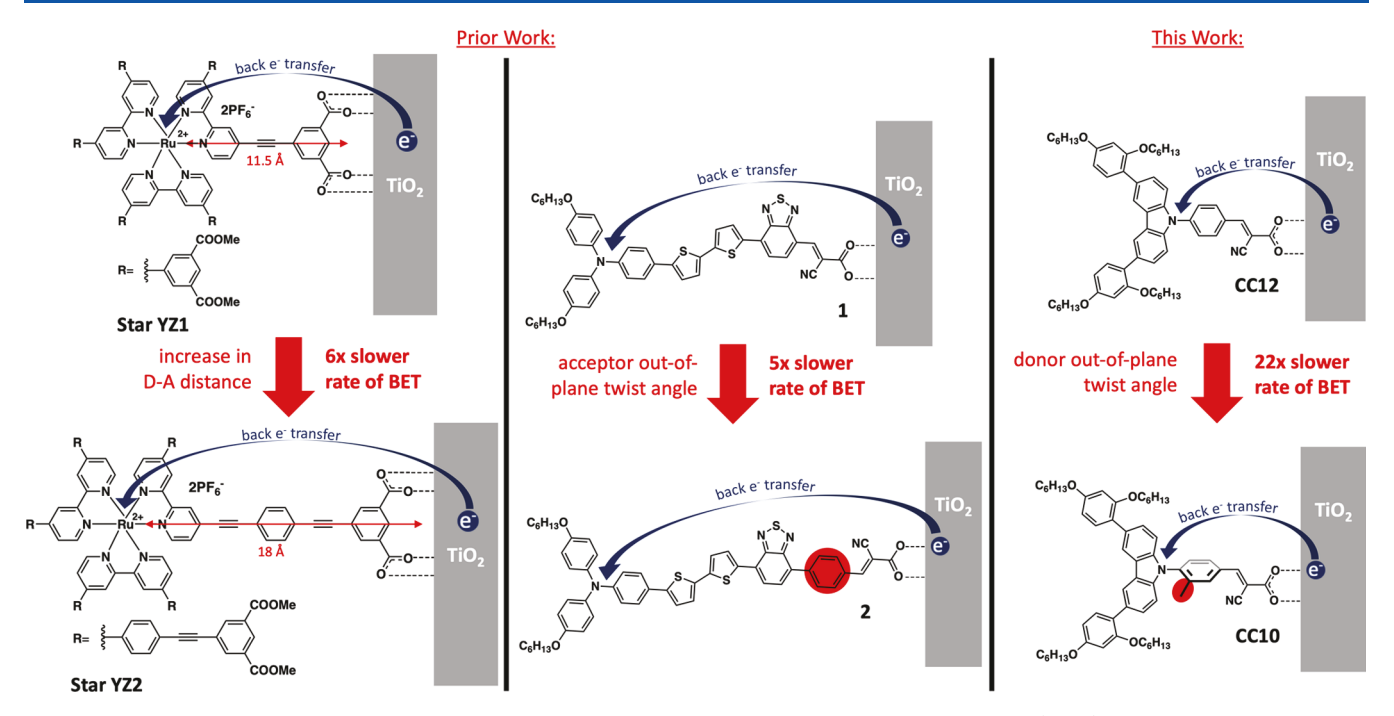


Figure 1. Comparison of methods used to slow the rate of back electron transfers from the semiconductor (TiO₂) to the oxidized dye.

electron injection, allowing excited state electron relaxation to compete with productive electron transfer pathways, consequently lowering the performance of the DSC devices. The second example study targeted the effect of placing a phenyl group between the dye-conjugated π -system and the anchor group. 13 The authors observed a 5× slower BET rate with the addition of a phenyl group and proposed that an increased twist angle of the radical cation is the reason for the slower rate. The increased twist angle is thought to electronically decouple the π -conjugation in the dye between the oxidized donor and the anchor/semiconductor. This change led to a 6.5× increase in DSC power conversion efficiency, a higher open-circuit voltage (V_{oc}) , and a higher short-circuit current density (J_{sc}) . Based on these observations, this prior study correlates an increase in DSC performance and longer chargeseparated state lifetimes with electronically decoupling charges across an interface. This current study seeks to probe the effect of sterically induced twist angles on the rate of BET through the addition of methyl groups on the donor region of the dye to produce twisted intramolecular charge-transfer systems. A series of three dyes were selected with increasing steric elements added as methyl groups to give CC12 (0 Me), CC10 (1 Me), and CC11 (2 Me) (Figure 1). Electronically decoupling the charges in the charge-separated state of the dye may lead to an increased charge-separated state lifetime and slow the rate of the BET reaction.

2. METHODS

2.1. General Information. Thin-layer chromatography (TLC) was conducted with Sorbent Technologies Silica XHL TLC plates with a UV254 indicator and visualized with a UV lamp. Manual flash column chromatography was performed with Sobtech silica gel technical grade P60, $40-63 \mu m$, (230–400 mesh), pH 6.0–8.0. CombiFlash column chromatography used Luknova SuperSep silica columns 30 mL/min, 50 μm , 200 psi, ranging from 4 to 80 g cartridges. ¹H and ¹³C NMR spectra were recorded on a Bruker Ascend-300 (300 MHz)

and a Bruker Ascend-400 (400 MHz) spectrometer and reported in ppm using solvent as an internal standard (CDCl₃ at 7.26 ppm). Singlet (s), doublet (d), doublet of doublets (dd), triplet (t), and multiplet (m) were used as ¹H NMR multiplicity patterns; J value coupling constants are in Hz. UV-vis spectra were recorded using an Avantes/AvaSpecULS2048-USB2-50 spectrometer (Pine Research part RRAVSP3) with an Avantes/AvaSpec light source (Pine Research part RRAVSP) and the AvaSoft8 software program. For electrospray ionization (ESI) high-resolution mass spectrometry (HRMS), quadruple-TOF was used to obtain the data, both in positive and negative modes, with a Waters Synapt HDMS or Orbitrap Exploris 240 to obtain the data in positive mode with a spray voltage of 3600 V, a resolution of 240,000, the ion transfer tube temperature set at 300 °C, and the mass analyzer set to the 200–2000 Da range. ATR-IR was taken using a Bruker Alpha Platinum-ATR FTIR spectrometer, and spectra were processed with OPUS 6.5 software. All IR samples were taken as a solid/neat unless otherwise noted. Electrochemical analysis via cyclic voltammetry was conducted with a CH Instruments potentiostat (CHI 600E). Electrochemical data is measured in dichloromethane (DCM) with a glassy carbon working electrode, a platinum wire counter electrode, a Ag wire pseudoreference electrode, and 0.1 M Bu₄NPF₆ as the electrolyte and referenced against ferrocenium/ferrocene (Fc+/Fc). All values are reported versus NHE with Fc⁺/Fc taken as 0.70 V versus NHE in DCM.^{23,24}

2.2. Nanosecond Transient Absorption Spectroscopy (nsTAS). TAS device fabrication: TiO_2 -dye films were prepared as previously reported, with modifications detailed herein.³⁷ The electrodes were composed of a single 3 μ m mesoporous, 30 nm particle-sized TiO_2 layer (Greatcell Solar Materials' 30NR-D Transparent Titania Paste, PN:002300). The layer was screen-printed from a Sefar screen (54/230-48W). The solution was composed of 0.3 mM dye in a 1:4 THF:EtOH solvent mixture with a 20:1 chenodeoxycholic acid (CDCA):dye ratio. The electrodes were washed with

acetonitrile, and the dried substrates were then partially sealed using two precut rectangles of a 25-µm-thick hot melt film (Surlyn, Solaronix, "Meltonix 1170-25") on either side of the electrodes' active area and topped with a thin glass coverslip (Corning cover glass thickness $1^{1}/_{2}$, $18 \times 18 \text{ mm}^{2}$) by heating the system to 130 °C under 0.1 psi pressure for 30 s. Devices were completed by filling the cells with an electrolyte solution by injection into the open portion using a microsyringe. The electrolyte was varied per device, as listed, with the following components: 0.5 M 4-tert-butylpyridine (TBP), 0.1 M lithium bis(trifluoromethanesulfonyl)imide (LiTFSI), 0.25 M Co-(bpy)₃²⁺, and 0.05 M Co(bpy)₃³⁺ in acetonitrile (MeCN). The remaining openings of the electrode are then sealed with a light-cured adhesive (Permabond UV6231) and cured under 405 nm light (390-420 nm emission base width) until hardened (~30 s) with the cell active dye area shielded from light using electrical tape.

Nanosecond transient absorption spectroscopy (TAS) measurements were performed using the Edinburgh LP980 optical system (Edinburgh Instruments, U.K.). Excitation (355 nm) light was generated from a pulsed Nd:YAG laser (Continuum, Surelite II) equipped with frequency-tripling crystal (<3 mJ/pulse, ~1 ns pulse width). The 355 nm laser pulse was then passed through a stilbene-based dye laser to generate 425 nm light pulsed excitation light. A 150 W pulsed xenon arc lamp was utilized as a probe. Time-resolved absorption decays were collected at the maximum of the excited-state absorption (650 nm for CC10 (1 Me) and CC11 (2 Me) and 660 nm for CC12 (0 Me)) by the use of a Czerny—Turner monochromator and a photomultiplier tube and averaged over 3000 laser shots. The following equations were used to obtain kinetics:

$$\Delta OD(t) = \Delta OD_{t=0} e^{-(\frac{t}{\tau_{KWW}})\beta}$$
(1)

where $\Delta \mathrm{OD}_{t=0}$ represents the signal amplitude at time zero, τ_{KWW} is the stretched exponential lifetime, and β is the stretch parameter, which ranges in value from 0 to 1. The observed lifetime is calculated from the fitting parameters using a gamma function distribution of β^{-1} (eqs 2 and 3).

$$\Gamma(x) = \int_0^\infty u^{(x-1)} e^{-x} du$$
 (2)

$$\tau_{obs} = \frac{\tau}{\beta} \Gamma \left(\frac{1}{\beta} \right) \tag{3}$$

To better account for biphasic kinetics, with competing rates of regeneration and BET, in the devices fabricated with CDCA, TBP, LiTFSI, and the $Co(bpy)_3^{3+/2+}$ redox shuttle, the ΔOD versus t curves were fit with a biexponential decay function

$$\Delta OD(t) = A_1 e^{-(x - x_0)/\tau_1} + A_2 e^{-(x - x_0)/\tau_2}$$
(4)

where A_1 and A_2 represent the weight of lifetimes τ_1 and τ_2 , respectively.⁴² From these lifetime values, an average lifetime $\tau_{\rm avg}$ was calculated by eq 5.

$$\tau_{\text{avg}} = \frac{A_1 \tau_1 + A_2 \tau_2}{A_1 + A_2} \tag{5}$$

2.3. Time-Correlated Single Photon Counting (TCSPC). Emission lifetime curves were obtained using the 405 nm line of an LDH series 405B pulsed diode laser (pulse width approximately 100 ps) as the excitation source, and emission was detected using a PicoQuant PDM series single

photon avalanche diode (time resolution approximately 50 ps) and a TimeHarp 260 time-correlated single photon counter (25 ps resolution). Appropriate filters were placed before the sample and detector. Time-resolved emission kinetics were best modeled by a double-exponential function. Fluorescence lifetime values were measured in dichloromethane.

2.4. Synthetic Proceedures. 2.4.1. tert-Butyl 4-(9H-Carbazol-9-yl)benzoate (3a). To a flame-dried, N2-gas-filled round-bottomed flask was added 2,2'-dibromo-1,1'-biphenyl (1, 4.00 g, 12.8 mmol, 1.0 equiv), methyl 4-aminobenzoate (2a, 2.32 g, 15.4 mmol, 1.2 equiv), sodium tert-butoxide (NaOt-Bu, 2.95 g, 30.8 mmol, 2.4 equiv), and toluene (51 mL, 0.25 M), followed by Pd₂(dba)₃ (0.587 g, 0.641 mmol, 5 mol %) and X-Phos (0.611 g, 1.28 mmol, 10 mol %). The roundbottomed flask was then sealed and heated to 100 °C. Upon completion by NMR, dichloromethane (DCM) and water were added to the reaction and the mixture was passed through Celite. The resulting DCM/water layers were then separated, and the DCM layer was washed with water three times. The DCM layer was then dried using anhydrous sodium sulfate (Na₂SO₄), and the solvent was removed under reduced pressure. The reaction was further purified using a CombiFlash automated column with a ramp of 100% hexanes to 50% DCM/50% hexanes followed by a methanol (MeOH) flush. Two products were formed and isolated, tert-butyl 4-(9Hcarbazol-9-yl)benzoate (3a, 27%) and methyl 4-(9H-carbazol-9-yl)benzoate (2%). The tert-butyl product was isolated as an off-white solid (3a, 1.20 g, 27% yield). ¹H NMR (400 MHz, chloroform-d) δ 8.24 (d, J = 8.4 Hz, 2H), 8.15 (d, J = 7.8 Hz, 2H), 7.65 (d, J = 8.4 Hz, 2H), 7.50–7.37 (m, 4H), 7.31 (t, J =7.3 Hz, 2H), 1.65 (s, 9H) ppm. ¹³C NMR (101 MHz, CDCl₃) δ 165.2, 141.7, 140.5, 131.3, 130.8, 126.4, 126.3, 123.9, 120.6, 109.9, 81.6, 28.4 ppm. IR (neat, cm⁻¹): 3061, 2973, 2934, 1709, 1601. HRMS (ESI-TOF) m/z calcd $[M + H]^+$ for C₂₃H₂₂NO₂: 344.1650; found: 344.1655.

2.4.2. Methyl 4-(9H-Carbazol-9-yl)-3-methylbenzoate (3b). To a flame-dried, N2-filled round-bottomed flask was added 2,2'-dibromo-1,1'-biphenyl (1, 4.00 g, 12.8 mmol, 1.0 equiv), methyl 4-amino-3-methylbenzoate (2b, 2.54 g, 15.4 mmol, 1.2 equiv), NaOt-Bu (2.95 g, 30.8 mmol, 2.4 equiv), and toluene (51 mL, 0.25 M) followed by the addition of Pd₂(dba)₃ (0.587 g, 0.641 mmol, 5 mol %), and X-Phos (0.611 g, 1.28 mmol, 10 mol %). The reaction was sealed and heated to 100 °C. Upon completion by NMR, dichloromethane (DCM) and water were added to the reaction and the mixture was passed through Celite. The resulting DCM/water layers were then separated, and the DCM layer was extracted with water three times. Following extraction, the DCM layer was dried using sodium sulfate (Na₂SO₄), and the solvent was removed under reduced pressure. The reaction was further purified using a CombiFlash automated column with a ramp of 100% hexanes to 60% DCM/40% hexanes and a MeOH flush. Two products were formed, tert-butyl 4-(9H-carbazol-9-yl)-3methylbenzoate (11%) and methyl 4-(9H-carbazol-9-yl)-3methylbenzoate (3b, 27%). The methyl product was isolated as an off-white solid (3b, 1.10 g, 27% yield). ¹H NMR (400 MHz, chloroform-d) δ 8.16 (d, J = 7.8 Hz, 3H), 8.07 (d, J =8.1 Hz, 1H), 7.46 (d, J = 8.1 Hz, 1H), 7.40 (t, J = 7.6 Hz, 2H), 7.30 (t, J = 7.4 Hz, 2H), 7.03 (d, J = 8.1 Hz, 2H), 3.99 (s, 3H), 2.05 (s, 3H) ppm. 13 C NMR (101 MHz, chloroform-d) δ 166.7, 140.8, 140.5, 137.7, 133.1, 130.4, 129.4, 128.7, 126.2, 123.4, 120.6, 120.1, 109.8, 52.5, 17.9 ppm. IR (neat, cm⁻¹)

3060, 2946, 2930, 1721. HRMS (ESI-TOF) m/z calcd [M + H]⁺ for $C_{21}H_{18}NO_2$: 316.1338; found: 316.1364.

2.4.3. Methyl 4-(9H-Carbazol-9-yl)-3,5-dimethylbenzoate (3c). To a flame-dried, N2-filled round-bottomed flask was added 2,2'-dibromo-1,1'-biphenyl (1, 5.50 g, 17.6 mmol, 1.0 equiv), methyl 4-amino-3,5-dimethylbenzoate (2c, 3.78 g, 21.2 mmol, 1.2 equiv), NaOt-Bu (4.06 g, 42.3 mmol, 2.4 equiv), and toluene (71 mL, 0.25M) followed by the addition of Pd₂(dba)₃ (0.807g, 0.882 mmol, 5 mol %) and X-Phos (0.841 g, 1.76 mmol, 10 mol %). The flask was sealed and heated to 100 °C. Upon completion by NMR, dichloromethane (DCM) and water were added to the reaction and the mixture was passed through Celite. The resulting DCM/water layers were then separated, and the DCM layer was washed with water three times. The DCM layer was then dried using anhydrous sodium sulfate (Na₂SO₄), and the solvent was removed under reduced pressure. The reaction was further purified using a CombiFlash automated column with a ramp of 100% hexanes to 60% DCM/40% hexanes and a MeOH flush. The methyl 4-(9H-carbazol-9-yl)-3,5-dimethylbenzoate product was isolated as an off-white solid (3c, 0.905 g, 16% yield). ¹H NMR (400 MHz, chloroform-d) δ 8.18 (d, J = 7.7 Hz, 2H), 7.96 (s, 2H), 7.39 (t, J = 7.6 Hz, 2H), 7.29 (t, J = 7.5 Hz, 2H), 6.90 (d, J =8.1 Hz, 2H), 3.99 (s, 3H), 1.92 (s, 6H) ppm. ¹³C NMR (101 MHz, chloroform-*d*) δ 167.0, 140.0, 139.1, 138.8, 130.4, 130.0, 126.3, 123.2, 120.7, 119.9, 109.4, 52.5, 17.7 ppm. IR (neat, cm⁻¹) 3055, 2949, 1720, 1625. HRMS (ESI-TOF) m/z calcd $[M + H]^+$ for $C_{22}H_{20}NO_2$: 330.1494; found: 330.1501.

2.4.4. tert-Butyl 4-(3,6-dibromo-9H-carbazol-9-yl)benzoate (4a). Compound 3a (1.00 g, 2.19 mmol, 1.0 equiv) and dimethylformamide (DMF, 14.6 mL, 0.20 M) were added to a flame-dried, N2-filled, round-bottomed flask and cooled to 0 °C. N-Bromosuccinimide (NBS, 1.23 g, 6.97 mmol, 2.2 equiv) was dissolved in minimal DMF and added dropwise to the reaction. Once complete, water was added to the reaction mixture, the mixture was extracted with DCM, the organic layer was dried with anhydrous Na2SO4, and the solvent was removed under reduced pressure. The organic layer was then further purified using a pad of silica gel and a solvent combination of 50% DCM/50% hexanes. The solvent was once again removed using reduced pressure to yield the product as an off-white solid (1.22 g, 84% yield). ¹H NMR (400 MHz, chloroform-d) δ 8.24 (d, J = 8.2 Hz, 2H), 8.20 (d, J = 8.2 Hz, 2H), 8 = 1.9 Hz, 2H), 7.58 (d, I = 8.4 Hz, 2H), 7.52 (dd, I = 8.7, 1.9)Hz, 2H), 7.29 (d, J = 8.7 Hz, 5H), 1.65 (s, 10H) ppm. ¹³C NMR (101 MHz, chloroform-d) δ 164.9, 140.6, 139.5, 131.5, 131.5, 129.7, 126.4, 124.4, 123.5, 113.7, 111.6, 81.8, 28.4 ppm. IR (neat, cm⁻¹) 3073, 2952, 1715, 1604. HRMS (ESI-TOF) (negative mode) m/z calcd [M]⁻ for $C_{23}H_{18}Br_2NO_2$: 499.9685; found: 499.9714.

2.4.5. Methyl 4-(3,6-Dibromo-9H-carbazol-9-yl)-3-methylbenzoate (4b). Compound 3b (1.00 g, 3.17 mmol, 1.0 equiv) and DMF (15.9 mL, 0.20 M) were added to a flamedried, N₂-filled, round-bottomed flask and cooled to 0 °C. NBS (1.23 g, 6.97 mmol, 2.2 equiv) was dissolved in minimal DMF and added dropwise to the reaction. (Note: The product was later identified as the white precipitate that forms in the reaction. Please refer to 4c for a more concise purification method.) Once complete, water was added to the reaction mixture, and then the mixture was extracted using DCM; however, the precipitated product did not readily solubilize in the organic layer. The organic layer was dried using Na₂SO₄ (onto which the product was adsorbed), and the liquid was

discarded. To separate the product from Na₂SO₄, the mixture of Na₂SO₄ and the precipitated product was extracted with DCM using a Soxhlet extractor over 3 days. The product was isolated as an off-white solid (1.30 g, 87% yield). ¹H NMR (400 MHz, chloroform-d) δ 8.22 (d, J = 1.9 Hz, 2H), 8.16 (s, 1H), 8.07 (dd, J = 8.1, 2.0 Hz, 1H), 7.50 (dd, J = 8.7, 2.0 Hz, 2H), 7.41 (d, J = 8.1 Hz, 1H), 6.89 (d, J = 8.7 Hz, 2H), 3.99 (s, 3H), 1.99 (s, 3H) ppm. ¹³C NMR (101 MHz, chloroform-d) δ 166.5, 139.8, 139.5, 137.5, 133.3, 131.1, 129.7, 129.3, 128.9, 124.0, 123.6, 113.4, 111.5, 52.6, 17.7 ppm. IR (neat, cm⁻¹) 3072, 2947, 1712, 1606. HRMS (ESI-TOF) (negative mode) m/z calcd [M]⁻ for C₂₁H₁₄Br₂NO₂: 471.9372; found: 471.9388.

2.4.6. Methyl 4-(3,6-Dibromo-9H-carbazol-9-yl)-3,5-dimethylbenzoate (4c). Compound 3c (0.850 g, 2.58 mmol, 1.0 equiv) and DMF (13.0 mL, 0.20 M) were added to a flamedried, N2 filled, round-bottomed flask and cooled to 0 °C. NBS (1.01 g, 5.68 mmol, 2.2 equiv) was dissolved in minimal DMF and added dropwise to the reaction. Upon reaction completion verified by NMR, the reaction mixture was added dropwise to a saturated aqueous K₂CO₃ to precipitate the product out of solution. The precipitate was then vacuum filtered and allowed to dry. The product was isolated as a pink off-white solid (1.25) g, quantitative yield). 1 H NMR (400 MHz, chloroform-d) δ 8.24 (d, J = 1.5 Hz, 2H), 7.95 (s, 2H), 7.49 (dd, J = 8.6, 1.7 Hz, 2H), 6.78 (d, J = 8.6 Hz, 2H), 3.98 (s, 3H), 1.88 (s, 6H) ppm. 13 C NMR (101 MHz, chloroform-d) δ 166.7, 139.0, 138.5, 138.0, 131.0, 130.2, 129.9, 123.9, 123.7, 113.2, 111.1, 52.6, 17.6 ppm. IR (neat, cm⁻¹) 3072, 2947, 1712, 1606 ppm. HRMS (ESI-TOF) (negative mode) m/z calcd [M]⁻ for C₂₂H₁₆Br₂NO₂: 485.9531; found: 485.9529.

2.4.7. tert-Butyl 4-(3,6-Bis(2,4-bis(hexyloxy)phenyl)-9Hcarbazol-9-yl)benzoate (6a). Compound 4a (1.20 g, 2.39 mmol, 1.0 equiv), (2,4-bis(hexyloxy)phenyl)boronic acid (1.93 g, 5.99 mmol, 2.5 equiv), potassium phosphate tribasic (1.52 g, 7.18 mmol, 3.0 equiv), and toluene:H₂O (48 mL:2.0 mL, 0.050 M:1.2 M) were added to a pressure flask and bubbled with N_2 . Tris(dibenzylideneacetone)dipalladium(0) (0.110 g, 0.120 mmol, 0.05 equiv) and X-Phos (0.282 g, 0.599 mmol, 0.25 equiv) were then added to the pressure flask. The pressure flask was sealed, and the reaction was allowed to run at 80 °C. After the starting material was consumed according to thin-layer chromatography (TLC), water was added to the reaction mixture, and the mixture was extracted using DCM. The organic layer was then dried with anhydrous Na₂SO₄ and the solvent was removed under reduced pressure. A CombiFlash automated column was run using a ramp of 100% hexanes to 100% toluene to yield the purified product (0.611 g, 29% yield). 1 H NMR (400 MHz, chloroform-d) δ 8.29-8.21 (m, 4H), 7.72 (d, J = 8.5 Hz, 2H), 7.59 (dd, J = 8.6, 1.3 Hz, 2H), 7.47 (d, I = 8.5 Hz, 2H), 7.35 (d, I = 9.0 Hz, 2H), 6.63-6.56 (m, 4H), 4.02 (t, J = 6.6 Hz, 4H), 3.97 (t, J = 6.4Hz, 4H), 1.88-1.78 (m, 4H), 1.77-1.68 (m, 4H), 1.66 (s, 9H), 1.53-1.45 (m, 4H), 1.44-1.33 (m, 12H), 1.30-1.16 (m, 8H), 0.99-0.88 (m, 6H), 0.82-0.72 (m, 6H) ppm. ¹³C NMR (101 MHz, chloroform-d) δ 165.3, 159.6, 157.2, 142.1, 139.5, 131.5, 131.3, 131.1, 130.4, 128.1, 126.2, 124.3, 124.1, 121.3, 109.1, 105.5, 100.7, 81.5, 68.6, 68.3, 31.8, 31.6, 29.5, 29.3, 28.4, 26.0, 25.9, 22.8, 22.7, 14.2, 14.1 ppm. IR (neat, cm⁻¹) 2929, 2858, 1712, 1604. HRMS (ESI-TOF) (positive mode) m/zcalcd $[M + H]^+$ for $C_{59}H_{78}NO_6$: 896.5829; found: 896.5880.

2.4.8. Methyl 4-(3,6-Bis(2,4-bis(hexyloxy)phenyl)-9H-car-bazol-9-yl)-3-methylbenzoate (6b). Compound 4b (1.23 g,

2.64 mmol, 1.0 equiv), (2,4-bis(hexyloxy)phenyl)boronic acid (2.13 g, 6.61 mmol, 2.5 equiv), potassium phosphate tribasic (1.68 g, 7.93 mmol, 3.0 equiv), and toluene:H₂O (53 mL:2.2 mL, 0.050 M:1.2 M) were added to a pressure flask and bubbled with N₂. Tris(dibenzylideneacetone)dipalladium(0) (0.121 g, 0.132 mmol, 0.05 equiv) and X-Phos (0.311 g, 0.661 mmol, 0.25 equiv) were then added to the pressure flask. The pressure flask was sealed, and the reaction was allowed to run at 80 °C. After the starting material was consumed according to thin-layer chromatography (TLC), water was added to the reaction mixture, and the mixture was extracted using DCM. The organic layer was then dried with anhydrous Na₂SO₄, and the solvent was removed under reduced pressure. A CombiFlash automated column was run using a ramp of 100% hexanes to 100% toluene to yield the purified product (0.253 g, 11% yield). 1 H NMR (400 MHz, chloroform-d) δ 8.28 (d, J = 1.6 Hz, 2H), 8.19 (s, 1H), 8.08 (dd, J = 8.1, 2.0 Hz, 1H), 7.57 (dd, J = 8.5, 1.7 Hz, 2H), 7.51 (d, J = 8.2 Hz, 1H), 7.35 (d, J = 8.9 Hz, 2H), 7.02 (d, J = 8.5 Hz, 2H), 6.64– 6.53 (m, 4H), 4.05–3.94 (m, 8H), 2.15 (s, 3H), 1.86–1.77 (m, 4H), 1.76–1.67 (m, 4H), 1.53–1.46 (m, 2H), 1.43–1.32 (m, 11H), 1.29–1.17 (m, 9H), 0.92 (q, J = 8.4, 7.6 Hz, 8H), 0.76 (t, J = 6.8 Hz, 6H) ppm. ¹³C NMR (101 MHz, chloroform-d) δ 166.9, 159.5, 157.2, 141.0, 140.0, 137.7, 133.1, 131.6, 130.6, 130.2, 129.4, 128.6, 128.0, 124.3, 123.7, 121.4, 109.1, 105.5, 100.7, 68.6, 68.3, 52.5, 31.8, 31.6, 29.5, 29.3, 26.0, 25.9, 22.8, 22.7, 18.1, 14.2, 14.1 ppm. IR (neat, cm⁻¹) 2927, 2857, 1723, 1606. HRMS (ESI-TOF) (positive mode) m/zcalcd $[M + H]^+$ for $C_{57}H_{74}NO_6$: 868.5516; found: 868.5518.

2.4.9. Methyl 4-(3,6-Bis(2,4-bis(hexyloxy)phenyl)-9H-carbazol-9-yl)-3,5-dimethylbenzoate (6c). Compound 4c (1.20 g, 2.46 mmol, 1.0 equiv), (2,4-bis(hexyloxy)phenyl)boronic acid (1.98 g, 6.16 mmol, 2.5 equiv), potassium phosphate tribasic (1.57 g, 7.39 mmol, 3.00 equiv), and toluene:H₂O (49 mL:2.1 mL, 0.050 M:1.2 M) were added to a pressure flask and bubbled with N₂. Tris(dibenzylideneacetone)dipalladium(0) (0.113 g, 0.123 mmol, 0.05 equiv) and X-Phos (0.30 g, 0.62 mmol, 0.25 equiv) were then added to the pressure flask. The pressure flask was sealed, and the reaction was allowed to run at 80 °C. After the starting material was consumed according to thin-layer chromatography (TLC), water was added to the reaction mixture, and the mixture was extracted using DCM. The organic layer was then dried with anhydrous Na₂SO₄, and the solvent was removed under reduced pressure. A CombiFlash automated column was run using a ramp of 100% hexanes to 100% toluene to yield the purified product (0.481 g, 22% yield). 1 H NMR (400 MHz, chloroform-d) δ 8.30 (d, J = 1.6 Hz, 2H), 7.98 (s, 2H), 7.56 (dd, J = 8.5, 1.7 Hz, 2H), 7.36 (d, J = 9.0 Hz, 2H), 6.88 (d, J = 8.4 Hz, 2H), 6.62-6.55 (m, 4H), 4.10-3.89 (m, 8H), 2.00 (s, 6H), 1.88-1.77 (m, 4H), 1.77–1.67 (m, 4H), 1.53–1.46 (m, 4H), 1.44– 1.32 (m, 12H), 1.30–1.15 (m, 8H), 0.98–0.88 (m, 6H), 0.81-0.68 (m, 6H) ppm. ¹³C NMR (101 MHz, chloroform-d) δ 167.1, 159.5, 157.1, 139.5, 139.1, 138.9, 131.6, 130.3, 130.3, 130.0, 128.1, 124.4, 123.5, 121.5, 108.6, 105.5, 100.7, 68.6, 68.3, 52.4, 31.8, 31.6, 29.5, 29.3, 26.0, 25.9, 22.8, 22.7, 17.9, 14.2, 14.1 ppm. IR (neat, cm⁻¹) 2925, 2857, 1724, 1606. HRMS (ESI-TOF) (positive mode) m/z calcd $[M + H]^+$ for C₅₈H₇₆NO₆: 882.5673; found: 882.5665.

2.4.10. (4-(3,6-Bis(2,4-bis(hexyloxy)phenyl)-9H-carbazol-9-yl)phenyl)methanol (7a). Compound 6a (0.420 g, 0.469 mmol, 1.0 equiv) dissolved in THF (minimal, 2.00 mL) was added to a dry round-bottomed flask placed in an $\rm N_2$

environment. The reaction was cooled to −78 °C, and lithium aluminum hydride (LAH) (3.05 mL, 3.05 mmol, 1.0 M in THF) was added dropwise. Once added, the mixture was allowed to warm up slowly to room temperature. Once the reaction was complete via NMR, the product was isolated following the Fieser workup: Dilute with 10 mL of diethyl ether (Et₂O) and cool to 0 $^{\circ}$ C. Slowly add 0.40 mL of H₂O. Add 0.40 mL of 15% NaOH_(aq). Add 1.20 mL of H₂O. Warm to room temperature and stir for 15 min. Add approximately 0.25 g of MgSO₄ and 0.10 g of Celite and stir for 15 min. The product was obtained by filtering through packed Celite to remove salts using DCM and Et₂O. The product was used with no further purification (0.174 g, 61% yield). ¹H NMR (400 MHz, chloroform-*d*) δ 8.26 (s, 2H), 7.63 (s, 4H), 7.57 (dd, J =8.5, 1.7 Hz, 2H), 7.40 (d, J = 8.5 Hz, 2H), 7.35 (d, J = 8.9 Hz, 2H), 6.63-6.55 (m, 4H), 4.85 (s, 2H), 4.01 (t, J = 6.5 Hz, 4H), 3.97 (t, J = 6.4 Hz, 4H), 1.88-1.76 (m, 4H), 1.77-1.65(m, 4H), 1.54–1.46 (m, 4H), 1.45–1.30 (m, 12H), 1.29–1.17 (m, 8H), 0.98-0.87 (m, 6H), 0.81-0.72 (m, 6H) ppm. ¹³CNMR (75 MHz, chloroform-d) δ 159.5, 157.2, 140.0, 139.9, 137.6, 131.5, 130.6, 128.6, 127.9, 127.2, 124.4, 123.7, 121.2, 109.1, 105.5, 100.8, 68.6, 68.3, 65.1, 31.8, 31.7, 29.5, 29.3, 26.0, 25.9, 22.8, 22.7, 14.2, 14.1 ppm. IR (neat, cm⁻¹) 2927, 2857, 1606. HRMS (ESI-TOF) (positive mode) m/z calcd [M + H]⁺ for C₅₅H₇₂NO₅: 826.5434; found: 826.5411.

2.4.11. (4-(3,6-Bis(2,4-bis(hexyloxy)phenyl)-9H-carbazol-9-yl)-3-methylphenyl)methanol (7b). Compound 6b (0.167 g, 0.192 mmol, 1.0 equiv) dissolved in THF (minimal, 2.0 mL) was added to a dry round-bottomed flask placed in an N₂ environment. The reaction was cooled to −78 °C, and LAH (1.25 mL, 1.25 mmol, 1.0 M in THF) was added dropwise. Once added, the mixture was allowed to warm up slowly to room temperature. Once the reaction was complete via NMR, the product was isolated following the Fieser workup: Dilute with 10 mL of diethyl ether (Et₂O) and cool to 0 °C. Slowly add 0.20 mL H₂O. Add 0.20 mL of 15% NaOH_(aq). Add 1.0 mL of H₂O. Warm to room temperature and stir for 15 min. Add approximately 0.25 g of MgSO₄ and 0.10 g of Celite and stir for 15 min. The product was obtained by filtering through packed Celite to remove salts using DCM and Et₂O. The product was used with no further purification (0.110 g, 68% yield). ¹H NMR (300 MHz, chloroform-d) δ 8.28 (d, J = 1.3Hz, 2H), 7.55 (dd, J = 8.5, 1.7 Hz, 2H), 7.50 (s, 1H), 7.41 (d, J= 1.0 Hz, 2H), 7.35 (d, J = 9.0 Hz, 2H), 7.02 (d, J = 8.5 Hz,2H), 6.66-6.54 (m, 4H), 4.83 (s, 2H), 4.06-3.92 (m, 8H), 2.07 (s, 3H), 1.88–1.77 (m, 4H), 1.76–1.66 (m, 4H), 1.53– 1.42 (m, 4H), 1.42-1.30 (m, 12H), 1.29-1.16 (m, 8H), 0.99-0.87 (m, 6H), 0.81-0.68 (m, 6H) ppm. ¹³C NMR (101 MHz, chloroform-*d*) δ 159.4, 157.2, 141.2, 140.4, 137.8, 135.9, 131.6, 130.1, 129.6, 127.8, 127.8, 125.9, 124.5, 123.4, 121.3, 109.1, 105.5, 100.7, 68.6, 68.3, 65.2, 31.8, 31.7, 29.5, 29.3, 26.0, 25.9, 22.8, 22.7, 18.0, 14.2, 14.1 ppm. IR (neat, cm⁻¹) 2926, 2857, 1606. HRMS (ESI-TOF) (positive mode) m/z calcd [M]⁺ for C₅₆H₇₄NO₅: 840.5567; found: 840.5529.

2.4.12. (4-(3,6-Bis(2,4-bis(hexyloxy)phenyl)-9H-carbazol-9-yl)-3,5-dimethylphenyl)methanol (7c). Compound 6c (0.357 g, 0.405 mmol, 1.0 equiv) dissolved in THF (minimal, 2.0 mL) was added to a dry round-bottomed flask placed under an N_2 environment. The reaction was cooled to $-78\,^{\circ}$ C, and LAH (2.63 mL, 2.63 mmol, 1.0 M in THF) was added dropwise. Once added, the mixture was allowed to warm up slowly to room temperature. Once the reaction was complete via NMR, the product was isolated following the Fieser

workup: Dilute with 10 mL of diethyl ether (Et₂O) and cool to 0 °C. Slowly add 0.40 mL of H₂O. Add 0.35 mL of 15% NaOH_(aq). Add 1.0 mL of H₂O. Warm to room temperature and stir for 15 min. Add approximately 0.25 g of MgSO₄ and 0.10 g of Celite and stir for 15 min. The product was obtained by filtering through packed Celite to remove salts using DCM and Et₂O. The product was used with no further purification (0.280 g, 81% yield). ¹H NMR (300 MHz, chloroform-d) δ 8.29 (d, J = 1.3 Hz, 2H), 7.55 (dd, J = 8.5, 1.7 Hz, 2H), 7.37 (d, J = 9.0 Hz, 2H), 7.29 (s, 2H), 6.92 (d, J = 8.4 Hz, 2H),6.63-6.54 (m, 4H), 4.79 (s, 2H), 4.08-3.92 (m, 8H), 1.95 (s, 6H), 1.89–1.74 (m, 4H), 1.77–1.67 (m, 4H), 1.55–1.45 (m, 4H), 1.42-1.32 (m, 12H), 1.28-1.15 (m, 8H), 0.98-0.87 (m, 6H), 0.80-0.70 (m, 6H) ppm. ¹³C NMR (75 MHz, chloroform-d) δ 159.4, 157.1, 141.2, 139.5, 138.7, 134.4, 131.6, 129.9, 127.9, 127.3, 124.5, 123.3, 121.4, 108.8, 105.5, 100.7, 68.6, 68.3, 65.3, 31.8, 31.6, 29.5, 29.3, 26.0, 25.9, 22.8, 22.7, 17.9, 14.2, 14.1 ppm. IR (neat, cm⁻¹) 2953, 2859, 1606 ppm. HRMS (ESI-TOF) (positive mode) m/z calcd $[M + H]^+$ for C₅₇H₇₆NO₅: 854.5723; found: 854.5773.

2.4.13. 4-(3,6-Bis(2,4-bis(hexyloxy)phenyl)-9H-carbazol-9yl)benzaldehyde (8a). Compound 7a (0.157 g, 0.190 mmol, 1.0 equiv) dissolved in minimal DCM was placed in a dry, N₂filled round-bottomed flask and allowed to bubble with N₂. Dess-Martin periodinane (DMP, 0.161g, 0.380 mmol, 2.0 equiv) was added to the flask and allowed to stir at room temperature. The reaction was monitored using NMR. Once the reaction was complete, the reaction mixture was poured onto a pad of silica gel and flushed with diethyl ether and DCM to yield the product (0.112 g, 72% yield). ¹H NMR (400 MHz, chloroform-*d*) δ 10.12 (s, 1H), 8.26 (d, J = 1.7 Hz, 2H), 8.15 (d, J = 8.3 Hz, 2H), 7.86 (d, J = 8.2 Hz, 2H), 7.61 (dd, J =8.5, 1.7 Hz, 2H), 7.52 (d, J = 8.6 Hz, 2H), 7.35 (d, J = 8.9 Hz, 2H), 6.63-6.55 (m, 4H), 4.02 (t, J = 6.6 Hz, 4H), 3.97 (t, J =6.4 Hz, 4H), 1.86–1.77 (m, 4H), 1.76–1.67 (m, 4H), 1.52– 1.46 (m, 4H), 1.44–1.31 (m, 12H), 1.30–1.17 (m, 8H), 0.93 (t, J = 6.8 Hz, 6H), 0.76 (t, J = 6.9 Hz, 6H) ppm. ¹³C NMR (75 MHz, chloroform-d) δ 191.2, 159.7, 157.2, 144.0, 139.2, 134.5, 131.6, 131.5, 131.5, 128.2, 126.7, 124.4, 124.1, 121.4, 109.2, 105.6, 100.7, 68.6, 68.3, 31.8, 31.6, 29.5, 29.3, 26.0, 25.9, 22.8, 22.7, 14.2, 14.1 ppm. IR (neat) 2925, 2856, 1700. HRMS (ESI-TOF) (positive mode) m/z calcd $[M + Cs]^+$ for C₅₅H₆₉NO₅Cs: 956.4230; found: 956.4214.

2.4.14. 4-(3,6-Bis(2,4-bis(hexyloxy)phenyl)-9H-carbazol-9yl)-3-methylbenzaldehyde (8b). Compound 7b (0.0970 g, 0.115 mmol, 1.0 equiv) dissolved in minimal DCM was placed in a dry, N2-filled round-bottomed flask and allowed to bubble with N₂. DMP (0.098 g, 0.231 mmol, 2.0 equiv) was added to the flask and allowed to stir at room temperature. The reaction was monitored using NMR. Once the reaction was complete, the reaction mixture was poured onto a pad of silica gel and flushed with diethyl ether and DCM to yield the product (0.0773 g, 80% yield). ¹H NMR (400 MHz, chloroform-d) δ 10.14 (s, 1H), 8.28 (d, J = 1.7 Hz, 2H), 8.03 (s, 1H), 7.94 (dd, J = 8.1, 1.9 Hz, 1H), 7.62 (d, J = 8.0 Hz, 1H), 7.57 (dd, J = 8.5, 1.7 Hz, 2H), 7.35 (d, J = 9.0 Hz, 2H), 7.03 (d, J = 8.5 Hz, 2H),6.62-6.55 (m, 4H), 4.01 (t, J = 6.6 Hz, 4H), 3.97 (t, J = 6.4Hz, 4H), 2.19 (s, 3H), 1.87-1.76 (m, 4H), 1.77-1.66 (m, 4H), 1.54–1.45 (m, 4H), 1.45–1.31 (m, 12H), 1.30–1.16 (m, 8H), 0.96–0.87 (m, 6H), 0.80–0.72 (m, 6H) ppm. ¹³C NMR (75 MHz, chloroform-d) δ 191.7, 159.6, 157.2, 142.4, 139.8, 138.4, 136.2, 133.1, 131.5, 130.8, 130.1, 128.8, 128.1, 124.2, 123.8, 121.4, 109.1, 105.5, 100.7, 68.6, 68.3, 31.8, 31.6, 29.5,

29.3, 26.0, 25.9, 22.8, 22.7, 18.2, 14.2, 14.1 ppm. IR (neat, cm⁻¹) 2925, 2856, 1701, 1604 ppm. HRMS (ESI-TOF) (positive mode) m/z calcd [M + H]⁺ for $C_{56}H_{72}NO_5$: 838.5411; found: 838.5342.

2.4.15. 4-(3,6-Bis(2,4-bis(hexyloxy)phenyl)-9H-carbazol-9yl)-3,5-dimethylbenzaldehyde (8c). Compound 7c (0.250 g, 0.293 mmol, 1.0 equiv) dissolved in minimal DCM was placed in a dry, N2-filled round-bottomed flask and allowed to bubble with N_2 . DMP (0.248 g, 0.585 mmol, 2.0 equiv) was added to the flask and allowed to stir at room temperature. The reaction was monitored using NMR. Once the reaction was complete, the reaction mixture was poured onto a pad of silica gel and flushed with diethyl ether and DCM to yield the product (0.218 g, 87% yield). 1 H NMR (400 MHz, chloroform-d) δ 10.11 (s, 1H), 8.30 (d, J = 1.6 Hz, 2H), 7.82 (s, 2H), 7.57 (dd, J = 8.4, 1.7 Hz, 2H), 7.36 (d, J = 9.0 Hz, 2H), 6.88 (d, J = 8.5Hz, 2H), 6.63-6.54 (m, 4H), 4.06-3.94 (m, 8H), 2.04 (s, 6H), 1.88-1.76 (m, 4H), 1.78-1.67 (m, 4H), 1.54-1.46 (m, 4H), 1.45–1.31 (m, 12H), 1.28–1.15 (m, 8H), 0.97–0.88 (m, 6H), 0.80-0.68 (m, 6H) ppm. ¹³C NMR (101 MHz, chloroform-d) δ 192.1, 159.5, 157.1, 140.9, 139.8, 139.0, 136.3, 131.5, 130.5, 130.1, 128.1, 124.3, 123.6, 121.5, 108.6, 105.5, 100.7, 68.6, 68.3, 31.8, 31.6, 29.5, 29.3, 26.0, 25.9, 22.8, 22.7, 18.0, 14.2, 14.1 ppm. IR (neat, cm⁻¹) 2925, 2857, 1700, 1605. HRMS (ESI-TOF) (positive mode) m/z calcd $[M + H]^+$ for C₅₇H₇₃NO₅: 852.5567; found: 852.5521.

2.4.16. (E)-3-(4-(3,6-Bis(2,4-bis(hexyloxy)phenyl)-9H-carbazol-9-yl)phenyl)-2-cyanoacrylic acid (CC12). Compound 8a (15 mg, 0.0182 mmol, 1.0 equiv) was added to a dry, N_2 filled pressure vessel with N₁N-dimethylformamide (DMF, 0.182 mL, 0.10 M), triphenylphosphine (PPh₃, 0.94 mg, 0.0036 mmol, 0.2 equiv), and cyanoacetic acid (2.0 mg, 0.0237 mmol, 1.3 equiv). The reaction was sealed and stirred at 75 $^{\circ}$ C. Hünig's base (N,N-diisopropylethylamine) (4 μ L, 0.0237 mmol, 1.3 equiv) was added to the reaction after 1 h. Water was added to the reaction mixture, the mixture was extracted using DCM, the water was discarded, and the DCM was removed under reduced pressure. The product was obtained using a pad of silica gel using 100% DCM, followed by a range of 1% MeOH/99% DCM to 20%MeOH/80% DCM as a yellow solid (15 mg, 92% yield). ¹H NMR (300 MHz, chloroform-d) δ 8.37 (s, 1H), 8.33–8.24 (m, 4H), 7.85 (d, I =8.5 Hz, 2H), 7.62 (dd, J = 8.5, 1.7 Hz, 2H), 7.55 (d, J = 8.8 Hz, 2H), 7.35 (d, J = 8.9 Hz, 2H), 6.63-6.54 (m, 4H), 4.07-3.92(m, 8H), 1.88–1.58 (m, 12H), 1.43–1.15 (m, 20H), 1.00– 0.69 (m, 12H) ppm. IR (neat, cm⁻¹) 2923, 2854, 1727, 1604. HRMS (ESI-TOF) (negative mode) m/z calcd [M]⁻ for C₅₈H₆₉N₂O₆: 889.5156; found: 889.5145.

2.4.17. (E)-3-(4-(3,6-Bis(2,4-bis(hexyloxy)phenyl)-9H-carbazol-9-yl)-3-methylphenyl)-2-cyanoacrylic acid (CC10). Compound 8b (36.5 mg, 0.0435 mmol, 1.0 equiv), cyanoacetic acid (4.1 mg, 0.0478 mmol, 1.1 equiv), acetic acid (5.0 μ L, 0.087 mmol, 2.0 equiv), and 4-aminophenol (1.9 mg, 0.0174 mmol, 0.4 equiv) were added to a round-bottomed flask. Toluene (12.5 mL) was added, and a Dean–Stark apparatus was attached with a condenser open to air. After the starting material was consumed according to thin-layer chromatography (TLC), the reaction mixture solvent was removed under reduced pressure and DCM was added to the reaction mixture. The reaction mixture in DCM was then purified through a pad of silica gel using a solvent range of 100% DCM to 20% MeOH/80% DCM. The product was then extracted using DCM and water followed by concentration of the organics via

Figure 2. Structures of CC10-CC12.

Scheme 1. Synthetic Route for Dyes CC10-CC12^a

"Knoevenagel conditions for CC12: cyanoacetic acid, triphenylphosphine, and Hünig's base in dimethylformamide; CC10 and CC11: cyanoacetic acid and 4-aminophenol in toluene.

reduced pressure to yield the yellow product (26 mg, 66% yield). 1 H NMR (400 MHz, chloroform-d) δ 8.32 (s, 1H), 8.21 (s, 2H), 8.08–8.00 (m, 2H), 7.56–7.49 (m, 3H), 7.28 (d, J = 9.0 Hz, 2H), 6.98 (d, J = 8.5 Hz, 2H), 6.55–6.49 (m, 4H), 3.94 (t, J = 6.6 Hz, 4H), 3.90 (t, J = 6.4 Hz, 4H), 2.12 (s, 3H), 1.81–1.69 (m, 4H), 1.69–1.56 (m, 4H), 1.47–1.38 (m, 4H), 1.38–1.25 (m, 12H), 1.25–1.08 (m, 8H), 0.89–0.82 (m, 6H), 0.72–0.65 (m, 6H) ppm. IR (neat, cm $^{-1}$) 2922, 2853, 1664, 1605. HRMS (ESI-TOF) (negative mode) m/z calcd [M] $^{-1}$ for $C_{59}H_{71}N_2O_6$: 903.5312; found: 903.5325.

2.4.18. (E)-3-(4-(3,6-Bis(2,4-bis(hexyloxy)phenyl)-9H-carbazol-9-yl)-3,5-dimethylphenyl)-2-cyanoacrylic acid (CC11). Compound 8c (42.8 mg, 0.0502 mmol, 1.0 equiv), cyanoacetic acid (4.7 mg, 0.0552 mmol, 1.1 equiv), acetic acid (5.7 μ L, 0.1004 mmol, 2.0 equiv), and 4-aminophenol (2.2 mg, 0.0201 mmol, 0.4 equiv) were added to a round-bottomed flask. Toluene was added (12.5 mL), and a Dean–Stark apparatus was attached with a condenser open to air. After the starting material was consumed according to thin-layer chromatography (TLC), the reaction mixture solvent was

reduced by vacuum, and DCM was added. The reaction mixture in DCM was then purified through a pad of silica gel using a solvent range of 100% DCM to 20% MeOH/80% DCM. The product was then extracted using DCM and water, followed by concentration of the organics via reduced pressure to yield the yellow product (13 mg, 28% yield). 1 H NMR (300 MHz, chloroform-d) δ 8.35 (s, 1H), 8.30 (s, 2H), 7.96 (s, 2H), 7.57 (d, J = 7.0 Hz, 2H), 7.36 (d, J = 8.9 Hz, 2H), 6.90 (d, J = 8.0 Hz, 2H), 6.63–6.54 (m, 4H), 4.05–3.94 (m, 8H), 2.03 (s, 6H), 1.91–1.57 (m, 8H), 1.54–1.13 (m, 24H), 0.97–0.88 (m, 6H), 0.79–0.71 (m, 6H) ppm. IR (neat, cm $^{-1}$) 2923, 2854, 1719, 1665, 1607. HRMS (ESI-TOF) (negative mode) m/z calcd [M] $^{-1}$ for $C_{60}H_{73}N_2O_{6}$: 917.5469; found: 917.5428.

3. RESULTS AND DISCUSSION

Three dyes with carbazole-based donors were synthesized with varied numbers of methyl groups near the carbazole donor: CC12 (0 Me), CC10 (1 Me), and CC11 (2 Me), as shown in Figure 2. All of the dyes feature the same cyanoacrylic acid acceptor and carbazole-based donor with ortho- and para-alkyl ether groups on the aryl rings at the 3 and 6 positions of the carbazole. The cyanoacrylic acid acceptor was selected based on the literature evidence of strong binding to TiO₂. ^{17,18} The alkyl ether groups were implemented to guard against the possible unfavorable electron transfer reaction between the redox shuttle and the surface of TiO₂, commonly known as the recombination reaction.

CC10—CC12 were synthesized as depicted in Scheme 1 beginning with a Buchwald cross-coupling reaction of dibromo 1 and aniline derivative 2 to yield carbazole 3. Carbazole 3 is then brominated using an *N*-bromosuccinimide (NBS) to yield dibromocarbazole 4. A Suzuki cross-coupling reaction with 4 and boronic acid 5 yields alkylated carbazole 6. 6 then undergoes a lithium aluminum hydride (LAH) reduction to give alcohol 7, followed by a Dess-Martin periodinane (DMP) oxidation to yield aldehyde 8. Finally, aldehyde 8 undergoes a Knoevenagel condensation reaction to yield dyes CC10—CC12 (Scheme 1).

The optical properties of CC10–CC12 were studied in solution and on the surface of TiO₂ by UV–vis absorption spectroscopy (Figures 3, S2, and S4 and Table 1). The effect of the structural changes between the dyes is observable from the solution measurements in dichloromethane (DCM). The trend observed with the dye series based on the maximum absorption wavelength ($\lambda_{\rm max}$) was CC11 (2 Me) < CC10 (1 Me) < CC12 (0 Me). The dye with the highest energy $\lambda_{\rm max}$

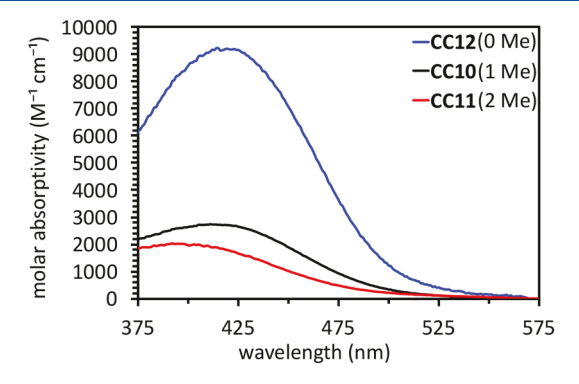


Figure 3. Molar absorptivity versus wavelength plot of dyes CC10-CC12 in DCM.

CC11 (2 Me), has two methyl groups, which suggests that this derivative would have the highest twist angle between the donor and acceptor in the series. Higher twist angles between the donor and acceptor are expected to weaken intramolecular charge transfer (ICT) and shift the absorption to higher energy. The trend in molar absorptivity follows the steric trend as well, with CC11 (2 Me) having the lowest molar absorptivity (ε) of 2,000 M⁻¹ cm⁻¹, followed by CC10 (1 Me) at 2,700 M⁻¹ cm⁻¹ and CC12 (0 Me) at 9,100 M⁻¹ cm⁻¹. The trends observed suggest the sterics modulating the planarity of the π -system have a substantial effect on dye optical properties as anticipated. Additionally, when comparing the absorption spectra of the dyes in solution versus on the surface of TiO₂, no significant variation is observed, suggesting that surface aggregation is not present (Figures S2–S4).

Dye electrochemical measurements were taken to confirm favorable electron transfer free energies from [Co(bpy)₃]- $[PF_6]_2$ to an oxidized dye and to TiO_2 from a photoexcited dye (Figures 4 and S1 and Table 1). $[Co(bpy)_3][PF_6]_2$ is a common redox mediator used with a wide range of dyes in the dye sensitization literature and serves as a benchmarking material for electron transfer reactions in this study. 20,26-The cyclic voltammograms of CC10-CC12 were all reversible, with a negligible difference in the oxidation potential of each dye. This indicates that the changes in sterics between the dyes does not have a major effect on the ground-state oxidation potential $(E_{(s+/s)})$. The $E_{(s+/s)}$ values of the dyes show favorable free energies of approximately 760 mV for the electron transfer reaction from $[Co(bpy)_3]^{2+}$ to the oxidized dye when the redox potential of $[Co(bpy)_3]^{2+}$ is taken as 0.56 V versus NHE.²⁰ The energy gap of each dye was found using the "0nset" program,²⁵ from which the excited-state oxidation potential ($E_{(s+/s^*)}$) for each dye was then calculated. $E_{(s+/s^*)}$ was calculated as explained in the literature.³⁰ The $E_{(s+/s^*)}$ of the dyes has a 120 mV difference among the dyes, following the trend of increasing sterics: CC12 (0 Me) > CC10 (1 Me) > CC11 (2 Me). The free energy for injection is adequate for each of the photoexcited dyes to transfer electrons to TiO2, with free energies ranging between 630 and 750 mV when TiO₂ is taken at -0.5 V versus NHE.³¹

Density functional theory (DFT) geometry optimizations and time-dependent density functional theory (TD-DFT) calculations were performed with the Gaussian 16 package.³² The M06-2X/6-311G (d,p) level of theory was used, 33,34 as recent literature found it to be accurate at estimating DSC dye absorption values. $^{35-37}$ In addition, functionals B3LYP and CAM-B3LYP were found to yield vertical transition values redshifted or blue-shifted, respectively, compared to M06-2X, which yielded the closest vertical transition values to correlate to the observed λ_{max} values. Table 2 summarizes the computational data obtained for the dye series. Each dye is observed to have orbital density located on the donor for the highest occupied molecular orbital (HOMO) and on the acceptor for the lowest unoccupied molecular orbital (LUMO) (Figure 5). The HOMO and LUMO orbitals are the highest contributors for the S_0 to S_1 transition for the neutral dyes at 87-89% (Table 2).

The vertical transition is observed to be close to the experimental absorption maxima for each dye with a difference of less than 0.20 eV. This reasonable agreement between experiment and theory suggests that this computational approach may be used for further analysis of the dyes. The dihedral angles (highlighted in Figure 5) at the junction of the

Table 1. Optical and Electrochemical Data for CC10-CC12 in DCM

	Absorbar	Electrochemical Data ^a			
Dye	λ_{\max} (nm)	$\lambda_{\text{onset}} (\text{nm})^b$	$\varepsilon \left(\mathrm{M^{-1}cm^{-1}} \right)$	$E_{(S+/S)}(V)^c$	$E_{(S+/S^*)}(V)^d$
CC12 (0 Me)	429	498	9,100	1.33	-1.13
CC10 (1 Me)	410	495	2,700	1.32	-1.19
CC11 (2 Me)	395	490	2,000	1.32	-1.25

"Measured with a glassy carbon working electrode, a Pt counter electrode, and an Ag wire pseudoreference electrode in 0.1 M tetrabutylammonium hexafluorophosphate (NBu₄PF₆) as the electrolyte. Ferrocenium/ferrocene is used as a reference taken as 0.70 V versus the normal hydrogen electrode (NHE). ^{23,24} ^b Absorption onset taken from the *x*-axis intercept of a line of best fit on the absorption curve on the low-energy side as calculated by the "Onset" program. ²⁵ ^c Measured via cyclic voltammetry (CV, Figure S1). ^d Calculated from the equation $E_{(S+/S^*)} = E_{(S+/S)} - E_g^{\text{opt}}$, where $E_g^{\text{opt}} = 1240/\lambda_{\text{onset}}$.

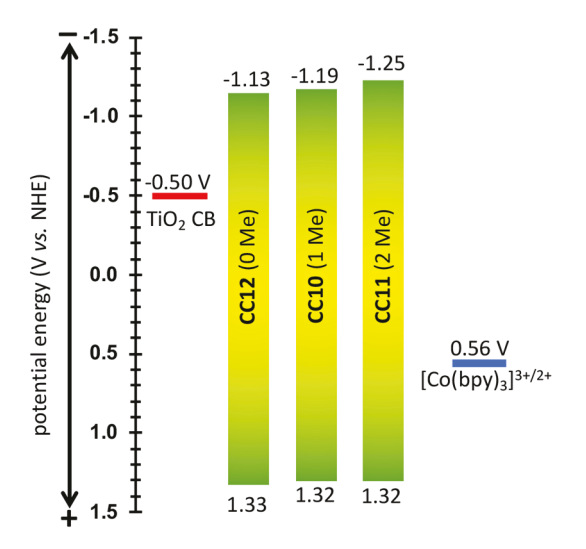


Figure 4. Energy-level diagram of dyes CC10-CC12.

donor to the acceptor portions of the dyes were obtained for each dye from the optimized geometries (Figure 5). As expected, the dihedral angle between the plane of the carbazole and the plane of the adjacent phenyl ring with a varied number of methyl groups increases as the steric environment increases via the addition of methyl groups on the phenyl ring. The dye dihedral angles increase as the sterics increase, with a 16° angle increase from CC12 (0 Me) to CC10 (1 Me) and a 11° increase from CC10 (1 Me) to CC11 (2 Me). The cationic dye geometries were optimized at the same level of theory. The change in dihedral angles between the neutral and cationic dyes is minor, with an increase in dihedral angle present for the cationic state (between 5 and 7°). The computational data suggests that as dye sterics increase the dihedral angle between the donor and acceptor also increases, particularly in the charge-separated state. We hypothesized this could aid in increasing charge-separated lifetimes across a TiO2 interface

and therefore pursued time-resolved studies to probe this concept.

Transient absorption spectroscopy (TAS) was used to measure the rate of the BET reaction and dye regeneration reaction. To probe the BET reaction, TAS electrodes were constructed using dye solutions composed of a 20:1 chenodeoxycholic acid (CDCA):dye ratio to minimize aggregation and an inert redox-inactive electrolyte solution composed of 0.5 M 4-tert-butylpyridine (TBP) and 0.1 M lithium bis(trifluoromethanesulfonyl)imide (LiTFSI) in acetonitrile (MeCN). The BET reaction is studied by first photoinducing interfacial charge separation (eq 6) and then monitoring the lifetime of the signal of the dye cation that is consumed in the BET reactions (eq 7).

$$dye|TiO_2 + h\nu \rightarrow dye^+|TiO_2(e^-)$$
 (6)

$$dye^{+}|TiO_{2}(e^{-}) \rightarrow dye|TiO_{2} \tag{7}$$

Long lifetimes for the BET reaction are favorable and are hypothesized to increase as the sterics of the dyes increase, due to the increase in dihedral angle strain observed with computational data. The following trend was observed for the lifetime of the interfacial charge-separated state: CC10 (1 Me) > CC11 (2 Me) > CC12 (0 Me) (Table 3, Table S2, Figure 6, and Figure S39). This trend reveals that compared to CC12 (0 Me), CC10 (1 Me) had a 22× longer lifetime, but interestingly, the lifetime decreases when implementing more sterics with CC11 (2 Me), leading to only a 1.6× lifetime increase. The origin of the shorter-than-expected lifetime for the charge-separated state at TiO₂ with CC11 (2 Me) is not apparent.

To observe the reaction rate for electron transfer from a redox mediator ($[Co(bpy)_3][PF_6]_2$) to the oxidized dye (eq 8), TAS electrodes were fabricated using the same dye solutions as above but with a redox-active electrolyte solution containing the components mentioned above with the addition

Table 2. Computational Data from DFT and TD-DFT Analysis of CC10-CC12

Dye	Orbitals $(S_0 \rightarrow S_1)$	% Cont.	Vert. Trans. (nmleV)	$\Delta E (eV)^a$	Osc. Strength	Dihedral Angle (deg)	Δ Dihedral $(deg)^b$
CC12 (0 Me)	$H \rightarrow L$	87%	394 3.14	0.19	0.5796	46°	+8
	$H-3 \rightarrow L$	8%					
CC10 (1 Me)	$H \rightarrow L$	89%	401 3.09	0.10	0.2894	62°	+7
	$H-3 \rightarrow L$	7%					
CC11 (2 Me)	$H \rightarrow L$	89%	388 3.19	0.09	0.1315	73°	+5
	$H-3 \rightarrow L$	6%					

 $[^]a\Delta E$ is the difference in the vertical transition energy and the experimental absorption maxima. $^b\Delta D$ ihedral is the change in the dihedral angle from the neutral dye to the oxidized dye.

I

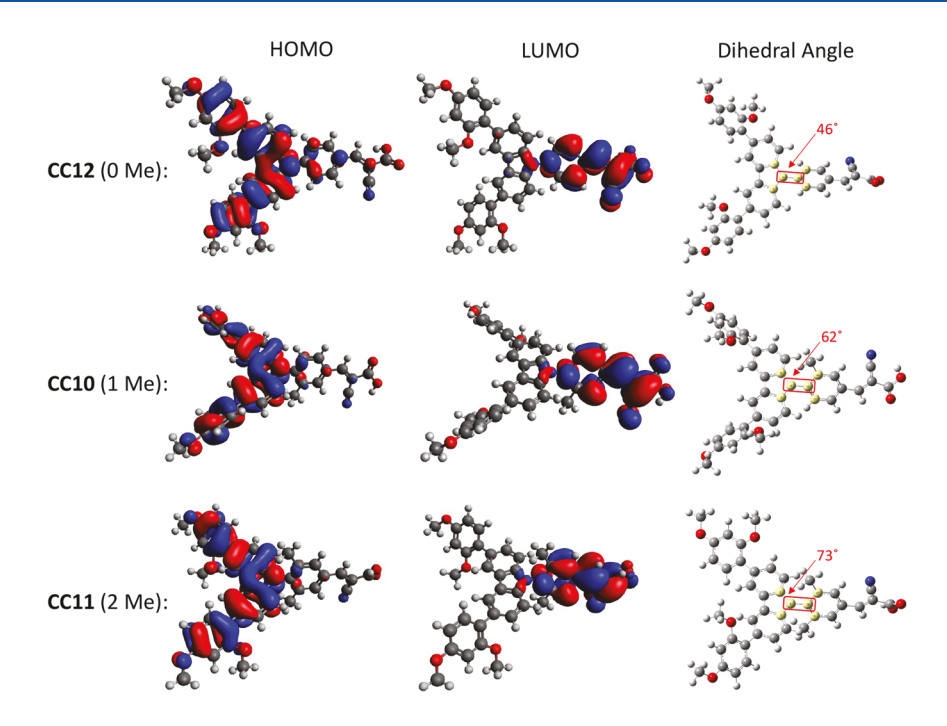


Figure 5. HOMOs, LUMOs, and dihedral angles for neutral dyes CC10-CC12 at the M06-2X/6-311G (d,p) level of theory. The dihedral angle analyzed is outlined in red along with the atoms involved in the angle highlighted in yellow.

Table 3. Comparison of TCSPC and nsTAS Lifetimes and Rates When Using Varied Components

Components	Experime	nt/Measurement	CC12 (0 Me)	CC10 (1 Me)	CC11 (2 Me)
${ m TiO_2}$ (inert electrolyte) a	TAS	$ au_{ m obs}~(\mu m s) \ k_{ m obs}~(m s^{-1}) \ m ratio~to~CC10$	17.1 5.48×10^4 0.05	368 2.71×10^3	26.6 3.76×10^{4} 0.07
${ m TiO_2}$ (active electrolyte) b	TAS	$ au_{ m avg}~(\mu { m s}) \ k_{ m avg}~({ m s}^{-1})$	0.03 0.70 1.43×10^6	2.02 4.95×10^{5}	1.52 6.58×10^{5}
DCM^c	TCSPC	ratio to CC10 τ_{avg} (ns)	0.35 1.7	1 2.7	0.75 1.9
		$k_{\rm obs}~({ m s}^{-1})$ ratio to CC10	5.88×10^8 0.63	3.70×10^{8}	5.26×10^8 0.70

[&]quot;Redox-inert electrolyte components include 0.5 M TBP, 0.1 M LiTFSI in MeCN, and a 20:1 ratio of CDCA:dye on TiO₂. ^bRedox-active electrolyte components include 0.5 M TBP, 0.1 M LiTFSI in MeCN, a 20:1 ratio of CDCA:dye on TiO₂, and 0.25 M/0.05 M Co(bpy)₃^{2+/3+}. ^cSolution components include 0.5 M TBP in DCM.

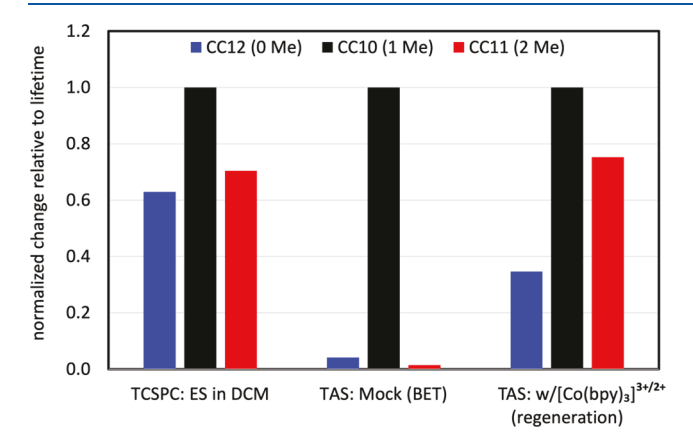


Figure 6. Normalized comparison of the lifetime of nsTAS and TCSPC with varied components using dyes CC10–CC12 on the surface of TiO₂ or in a DCM solution.

of a 0.05 M:0.25 M ratio of the $[Co(bpy)_3]^{3+/2+}$ redox shuttle (Figure 6, Figure S40, Table 3, and Table S3).

$$[Co(bpy)_3]^{2+} + dye^+|TiO_2(e^-) \rightarrow [Co(bpy)_3]^{3+} + dye|TiO_2(e^-)$$
(8)

It is common in the DSC literature to include both the 3+ and 2+ oxidation states of $Co(bpy)_3^{20,27-29}$ in the electrolyte at a ratio of 0.05 M Co³⁺:0.25 M Co²⁺. 26 [Co(bpy)₃]^{3+/2+} is added to the TAS devices to better mimic the environment of a functional DSC device. Shorter lifetimes for the redoxmediated electron transfer reaction are desired, as faster electron transfer to regenerate the neutral dye than BET is needed for high quantum yield systems. The rate trends observed with the introduction of $[Co(bpy)_3]^{3+/2+}$ remain the same as that of the BET reaction, with CC10 (1 Me) having the longest lifetime. However, the magnitude of change is only about 3× longer. Since the redox-mediated electron transfer reaction is in competition with the BET reaction and the BET reaction slows significantly more than the redox-mediated electron transfer reaction, the regeneration yield increases significantly with CC10 (1 Me) compared to CC12 (0 Me) and even CC11 (2 Me). Although CC10 (1 Me) has the longest regeneration lifetime, as shown in Table 3, it is only

1.32 μ s longer than CC12 (0 Me) and 0.5 μ s longer than CC11 (2 Me).

Time-correlated single photon counting (TCSPC) was taken to observe the lifetime of the excited state in solution (DCM) with 0.5 M TBP (Figure 6, Figure S38, Table 3, and Table S1). It is hypothesized that by increasing sterics on the dye, the charge-separated state becomes trapped, or more stable, and would therefore have a longer excited-state lifetime. The trend in the excited-state lifetime once again matches with the experiments mentioned above, where CC10 (1 Me) has the longest lifetime, followed by CC11 (2 Me), and CC12 (0 Me) has the shortest lifetime. Interestingly, CC12 (0 Me) and CC11 (2 Me) have very similar excited-state lifetimes while the lifetime of CC10 (1 Me) is almost double. The consistent trend in lifetime observed for the excited state, BET, and regeneration suggests overall agreement among the measurements where a balance between planarity and increased dihedral angle is reached for CC10 (1 Me). Interestingly, the trends do not agree with the hypothesis that larger steric hindrance leads to larger excited-state lifetimes and slower BET. Instead, these results suggest that a moderate twist angle leads to the most favorable outcomes with longer lifetimes for the BET reaction and excited-state lifetimes with a minor impact on the beneficial regeneration reaction.

DSC devices were fabricated with Co(bpy)₃^{2+/3+} as the redox shuttle, with and without a 20:1 ratio of CDCA:dye, to examine the effects of the kinetics probed in Table 3. The BET rate with CC10 is observed to be exceptionally slow in the series, which would promote higher device efficiencies if BET were problematic within functional devices. However, the regeneration rate is slowest for CC10, which would lead to lower-performing devices if this rate were problematic in devices. The current density-voltage (J-V), incident photonto-current conversion efficiency (IPCE), and small modulated photovoltage transient (SMPVT) measurements were evaluated for each dye, with and without CDCA (Table S4 and Figures S41-S46). The PCE values were calculated according to the equation PCE = $(J_{sc} \times V_{oc} \times FF)/I_0$, where J_{sc} is the short-circuit current density, $V_{\rm oc}$ is the open-circuit voltage, FF is the fill factor, and I_0 is the intensity of the incident light (1 sun, air mass 1.5G, 100 mW/cm², unless otherwise noted). The PCE values follow the trend of CC12 (0 Me) > CC10 (1 Me) > CC11 (2 Me) for the devices with and without CDCA, which suggests that the higher regeneration efficiency of CC12 may be an important factor in device performance (Table S4). IPCE curves reveal CC10 (1 Me) and CC12 (0 Me) to have an efficiency similar to those of CC10 (1 Me) having a peak efficiency of 40% and CC12 (0 Me) having a peak efficiency of 38% with no CDCA, while with CDCA both increase to have an IPCE peak of about 47% (Figures S43 and S44). Thus, despite the lower molar absorptivity of CC10 (1 Me), comparable IPCE values are observed which is likely because of the electrode thicknesses allowing for good light absorption from both photoanodes. Small modulated photovoltage transient (SMPVT) measurement DSC devices with dyes CC10-CC12 showed CC10 (1 Me) having a higher lifetime (less interfacial recombination) without CDCA, while with CDCA, CC12 (0 Me) had a higher lifetime, with CC11 (2 Me) having the lowest lifetime in both (Figures S45 and S46). The comparable performances of CC10 (1 Me) and CC12 (0 Me) in these devices suggest that for dyes that have poor performances in DSC devices or solar-to-fuel photoelectrochemical cell devices due to rapid BET, this strategy of a

twisted donor could be used to improve performance without a significant sacrifice of other device performance metrics.

4. CONCLUSIONS

Three dyes varying in sterics on the donor were analyzed for effects on the lifetime of the charge-separated state and consequently the BET reaction. nsTAS was used to determine the rates of the BET and regeneration reactions. The results revealed a 22× slower BET reaction rate using dye CC10 (1 Me) compared to the other dyes, CC12 (0 Me) and CC11 (2 Me). Although in the presence of a redox shuttle, as would be applicable to DSC devices, the rate of the regeneration reaction is slowed by about 3× with CC10 (1 Me). The TCSPC measurements revealed that the longest excited-state lifetime occurred with CC10 (1 Me), employing the one-methyl group. DSC devices showed comparable performaces for CC10 (1 Me) and CC12 (0 Me), which suggests adding moderate sterics does not negatively impact device performace while significantly slowing the BET reaction. These results suggest that moderate sterics, as in the case of CC10 (1 Me), lead to a more positive dramatic effect in the lifetime of the chargeseparated state than the utilization of lower sterics, CC12 (0 Me), or higher sterics, CC11 (2 Me). The key finding from this study is the need for balance when employing steric hindrance in dye design to yield favorable results.

ASSOCIATED CONTENT

Supporting Information

The Supporting Information is available free of charge at https://pubs.acs.org/doi/10.1021/acs.jpcc.3c04735.

Cyclic voltammetry, absorption spectroscopy data, NMR data, time-correlated single photon counting data, transient absorption data, and DSC device measurement data (PDF)

AUTHOR INFORMATION

Corresponding Author

Jared H. Delcamp — Department of Chemistry and
Biochemistry, University of Mississippi, University, Mississippi
38677, United States; Air Force Research Laboratories,
Materials & Manufacturing Directorate (RXNC), WrightPatterson Air Force Base, Ohio 45433, United States;
orcid.org/0000-0001-5313-4078; Email: delcamp@
olemiss.edu

Authors

Christine Curiac — Department of Chemistry and Biochemistry, University of Mississippi, University, Mississippi 38677, United States; orcid.org/0000-0003-2468-8906

Ethan C. Lambert — Department of Chemistry and
Biochemistry, University of Mississippi, University, Mississippi
38677, United States; Department of Chemistry and
Biochemistry, Florida State University, Tallahassee, Florida
32306, United States; orcid.org/0000-0001-6893-9071

Leigh Anna Hunt — Department of Chemistry and Biochemistry, University of Mississippi, University, Mississippi 38677, United States; Department of Chemistry, Ångström Laboratories, Uppsala University, SE 75120 Uppsala, Sweden; orcid.org/0000-0002-7681-3599

Mallory Roberts – Department of Chemistry and Biochemistry, University of Mississippi, University, Mississippi 38677, United States

- Ainsley LaMore Department of Chemistry and Biochemistry, University of Mississippi, University, Mississippi 38677, United States; Department of Chemistry, North Carolina State University, Raleigh, North Carolina 27606, United States
- Adithya Peddapuram Department of Chemistry and Biochemistry, University of Mississippi, University, Mississippi 38677, United States; Curia, AMRI (Albany Molecular Research Inc.), Albany, New York 12203, United States
- Hammad Cheema Department of Chemistry and Biochemistry, University of Mississippi, University, Mississippi 38677, United States; Archroma Inc. USA, Charlotte, North Carolina 28217, United States; ◎ orcid.org/0000-0002-7045-0141
- Nathan I. Hammer Department of Chemistry and Biochemistry, University of Mississippi, University, Mississippi 38677, United States; Occid.org/0000-0002-6221-2709

Complete contact information is available at: https://pubs.acs.org/10.1021/acs.jpcc.3c04735

Notes

The authors declare no competing financial interest.

ACKNOWLEDGMENTS

The dye synthesis and characterization studies (conducted by C.C., M.R., A.L., A.P., H.C., and J.H.D.) and DFT calculations (conducted by C.C. and J.H.D.) were supported by the U.S. Department of Energy, Office of Science, Office of Basic Energy Sciences, under award DE-SC0019131. TAS studies (conducted by E.C.L., L.A.H., and N.I.H.) were funded by the National Science Foundation award 1757220.

■ REFERENCES

- (1) Muñoz-García, A. B.; Benesperi, I.; Boschloo, G.; Concepcion, J. J.; Delcamp, J. H.; Gibson, E. A.; Meyer, G. J.; Pavone, M.; Pettersson, H.; Hagfeldt, A.; et al. Dye-Sensitized Solar Cells Strike Back. *Chem. Soc. Rev.* **2021**, *50* (22), 12450–12550.
- (2) Ren, Y.; Zhang, D.; Suo, J.; Cao, Y.; Eickemeyer, F. T.; Vlachopoulos, N.; Zakeeruddin, S. M.; Hagfeldt, A.; Grätzel, M. Hydroxamic Acid Preadsorption Raises Efficiency of Cosensitized Solar Cells. *Nature* **2023**, *613*, 60–65.
- (3) Boschloo, G. Improving the Performance of Dye-Sensitized Solar Cells. Front. Chem. 2019, 7, 77.
- (4) Zhang, S.; Yang, X.; Numata, Y.; Han, L. Highly Efficient Dye-Sensitized Solar Cells: Progress and Future Challenges. *Energy Environ. Sci.* **2013**, 6 (5), 1443.
- (5) Venkatesan, S.; Hsu, T.-H.; Teng, H.; Lee, Y.-L. Dye-Sensitized Solar Cells with Efficiency over 36% under Ambient Light Achieved by Cosensitized Tandem Structure. *Solar RRL* **2023**, *7*, 2300220.
- (6) Saygili, Y.; Söderberg, M.; Pellet, N.; Giordano, F.; Cao, Y.; Muñoz-García, A. B.; Zakeeruddin, S. M.; Vlachopoulos, N.; Pavone, M.; Boschloo, G.; Kavan, L.; Moser, J.-E.; Grätzel, M.; Hagfeldt, A.; Freitag, M. Copper Bipyridyl Redox Mediators for Dye-Sensitized Solar Cells with High Photovoltage. *J. Am. Chem. Soc.* **2016**, *138* (45), 15087—15096.
- (7) Saifullah, M.; Gwak, J.; Yun, J. H. Comprehensive Review on Material Requirements, Present Status, and Future Prospects for Building-Integrated Semitransparent Photovoltaics (BISTPV). J. Mater. Chem. A 2016, 4 (22), 8512–8540.
- (8) Lee, S.-H. A.; Zhao, Y.; Hernandez-Pagan, E. A.; Blasdel, L.; Youngblood, W. J.; Mallouk, T. E. Electron Transfer Kinetics in Water Splitting Dye-Sensitized Solar Cells Based on Core-Shell Oxide Electrodes. *Faraday Discuss.* **2012**, *155*, 165–176.
- (9) Johansson, P. G.; Kopecky, A.; Galoppini, E.; Meyer, G. J. Distance Dependent Electron Transfer at TiO ₂ Interfaces Sensitized

- with Phenylene Ethynylene Bridged Ru ^{II} -Isothiocyanate Compounds. J. Am. Chem. Soc. **2013**, 135 (22), 8331–8341.
- (10) Katz, M. J.; DeVries Vermeer, M. J.; Farha, O. K.; Pellin, M. J.; Hupp, J. T. Dynamics of Back Electron Transfer in Dye-Sensitized Solar Cells Featuring 4- *Tert* -Butyl-Pyridine and Atomic-Layer-Deposited Alumina as Surface Modifiers. *J. Phys. Chem. B* **2015**, *119* (24), 7162–7169.
- (11) Saavedra Becerril, V.; Franchi, D.; Abrahamsson, M. Ionic Liquid-Induced Local Charge Compensation: Effects on Back Electron-Transfer Rates in Dye-Sensitized TiO ₂ Thin Films. *J. Phys. Chem. C* **2016**, *120* (36), 20016–20023.
- (12) Hunt, L. A.; Rodrigues, R. R.; Foell, K.; Nugegoda, D.; Cheema, H.; Hammer, N. I.; Delcamp, J. H. Preferential Direction of Electron Transfers at a Dye-Metal Oxide Interface with an Insulating Fluorinated Self-Assembled Monolayer and MgO. *J. Phys. Chem.* C 2021, 125 (46), 25410–25421.
- (13) Haid, S.; Marszalek, M.; Mishra, A.; Wielopolski, M.; Teuscher, J.; Moser, J.-E.; Humphry-Baker, R.; Zakeeruddin, S. M.; Grätzel, M.; Bäuerle, P. Significant Improvement of Dye-Sensitized Solar Cell Performance by Small Structural Modification in π-Conjugated Donor-Acceptor Dyes. *Adv. Funct. Mater.* **2012**, 22 (6), 1291–1302.
- (14) Debnath, T.; Maity, P.; Lobo, H.; Singh, B.; Shankarling, G. S.; Ghosh, H. N. Extensive Reduction in Back Electron Transfer in Twisted Intramolecular Charge-Transfer (TICT) Coumarin-Dye-Sensitized TiO ₂ Nanoparticles/Film: A Femtosecond Transient Absorption Study. *Chem.—Eur. J.* **2014**, 20 (12), 3510–3519.
- (15) Morris, A. J.; Meyer, G. J. TiO ₂ Surface Functionalization to Control the Density of States. *J. Phys. Chem. C* **2008**, 112 (46), 18224–18231.
- (16) Johansson, P. G.; Zhang, Y.; Meyer, G. J.; Galoppini, E. Homoleptic "Star" Ru(II) Polypyridyl Complexes: Shielded Chromophores to Study Charge-Transfer at the Sensitizer-TiO ₂ Interface. *Inorg. Chem.* **2013**, 52 (14), 7947–7957.
- (17) Srinivas, K.; Yesudas, K.; Bhanuprakash, K.; Rao, V. J.; Giribabu, L. A Combined Experimental and Computational Investigation of Anthracene Based Sensitizers for DSSC: Comparison of Cyanoacrylic and Malonic Acid Electron Withdrawing Groups Binding onto the TiO $_2$ Anatase (101) Surface. *J. Phys. Chem. C* **2009**, 113 (46), 20117–20126.
- (18) Hara, K.; Tachibana, Y.; Ohga, Y.; Shinpo, A.; Suga, S.; Sayama, K.; Sugihara, H.; Arakawa, H. Dye-Sensitized Nanocrystalline TiO2 Solar Cells Based on Novel Coumarin Dyes. *Sol. Energy Mater. Sol. Cells* **2003**, 77 (1), 89–103.
- (19) Hagberg, D. P.; Jiang, X.; Gabrielsson, E.; Linder, M.; Marinado, T.; Brinck, T.; Hagfeldt, A.; Sun, L. Symmetric and Unsymmetric Donor Functionalization. Comparing Structural and Spectral Benefits of Chromophores for Dye-Sensitized Solar Cells. *J. Mater. Chem.* **2009**, *19* (39), 7232.
- (20) Feldt, S. M.; Gibson, E. A.; Gabrielsson, E.; Sun, L.; Boschloo, G.; Hagfeldt, A. Design of Organic Dyes and Cobalt Polypyridine Redox Mediators for High-Efficiency Dye-Sensitized Solar Cells. *J. Am. Chem. Soc.* **2010**, 132 (46), 16714–16724.
- (21) Huckaba, A. J.; Yella, A.; Brogdon, P.; Scott Murphy, J.; Nazeeruddin, M. K.; Grätzel, M.; Delcamp, J. H. A Low Recombination Rate Indolizine Sensitizer for Dye-Sensitized Solar Cells. *Chem. Commun.* **2016**, 52 (54), 8424–8427.
- (22) Curiac, C.; Rodrigues, R. R.; Watson, J.; Hunt, L. A.; Devdass, A.; Jurss, J. W.; Hammer, N. I.; Fortenberry, R. C.; Delcamp, J. H. Iron Redox Shuttles with Wide Optical Gap Dyes for High-Voltage Dye-Sensitized Solar Cells. *ChemSusChem* **2021**, *14* (15), 3084–3096.
- (23) Connelly, N. G.; Geiger, W. E. Chemical Redox Agents for Organometallic Chemistry. *Chem. Rev.* **1996**, *96* (2), 877–910.
- (24) Foltz, R. D. Handbook of Physics and Chemistry, 63rd ed.; CRC Press: Boca Raton, FL, 1982.
- (25) Wallace, A. M.; Curiac, C.; Delcamp, J. H.; Fortenberry, R. C. Accurate Determination of the Onset Wavelength (λ Onset) in Optical Spectroscopy. *Journal of Quantitative Spectroscopy and Radiative Transfer* **2021**, 265, 107544.

- (26) Li, L.; Xiao, J.; Sui, H.; Yang, X.; Zhang, W.; Li, X.; Hagfeldt, A.; Wu, M. Highly Effective Co3S4/Electrospun-Carbon-Nanofibers Composite Counter Electrode Synthesized with Electrospun Technique for Cobalt Redox Electrolyte Based on Dye-Sensitized Solar Cells. *J. Power Sources* **2016**, *326*, 6–13.
- (27) Mathew, S.; Yella, A.; Gao, P.; Humphry-Baker, R.; Curchod, B. F. E.; Ashari-Astani, N.; Tavernelli, I.; Rothlisberger, U.; Nazeeruddin, Md. K.; Grätzel, M. Dye-Sensitized Solar Cells with 13% Efficiency Achieved through the Molecular Engineering of Porphyrin Sensitizers. *Nature Chem.* **2014**, *6* (3), 242–247.
- (28) Feldt, S. M.; Wang, G.; Boschloo, G.; Hagfeldt, A. Effects of Driving Forces for Recombination and Regeneration on the Photovoltaic Performance of Dye-Sensitized Solar Cells Using Cobalt Polypyridine Redox Couples. *J. Phys. Chem. C* **2011**, *115* (43), 21500–21507.
- (29) Yella, A.; Lee, H.-W.; Tsao, H. N.; Yi, C.; Chandiran, A. K.; Nazeeruddin, Md. K.; Diau, E. W.-G.; Yeh, C.-Y.; Zakeeruddin, S. M.; Grätzel, M. Porphyrin-Sensitized Solar Cells with Cobalt (II/III)-Based Redox Electrolyte Exceed 12% Efficiency. *Science* **2011**, 334 (6056), 629–634.
- (30) Delcamp, J. H.; Yella, A.; Nazeeruddin, M. K.; Grätzel, M. Modulating Dye E(S+/S*) with Efficient Heterocyclic Nitrogen Containing Acceptors for DSCs. *Chem. Commun.* **2012**, 48 (17), 2295.
- (31) Rodrigues, R. R.; Peddapuram, A.; Dorris, A. L.; Hammer, N. I.; Delcamp, J. H. Thienopyrroledione-Based Photosensitizers as Strong Photoinduced Oxidants: Oxidation of Fe(Bpy) $_3$ $^{2+}$ in a > 1.3 V Dye-Sensitized Solar Cell. *ACS Appl. Energy Mater.* **2019**, 2 (8), 5547–5556.
- (32) Frisch, M. J.; Trucks, G. W.; Schlegel, H. B.; Scuseria, G. E.; Robb, M. A.; Cheeseman, J. R.; Scalmani, G.; Barone, V.; Petersson, G. A.; et al. *Gaussian 16*; Gaussian, Inc.: Wallingford, CT, 2016.
- (33) Zhao, Y.; Truhlar, D. G. The M06 Suite of Density Functionals for Main Group Thermochemistry, Thermochemical Kinetics, Noncovalent Interactions, Excited States, and Transition Elements: Two New Functionals and Systematic Testing of Four M06-Class Functionals and 12 Other Functionals. *Theor. Chem. Acc.* 2008, 120 (1–3), 215–241.
- (34) Frisch, M. J.; Pople, J. A.; Binkley, J. S. Self-consistent Molecular Orbital Methods 25. Supplementary Functions for Gaussian Basis Sets. *J. Chem. Phys.* **1984**, *80* (7), 3265–3269.
- (35) Alkhatib, Q.; Helal, W.; Afaneh, A. T. Assessment of Time-Dependent Density Functionals for the Electronic Excitation Energies of Organic Dyes Used in DSSCs. *New J. Chem.* **2022**, 46 (16), 7682–7694.
- (36) Liu, Y.; Luo, J. Performance of Time-Dependent Density Functional Theory on Twisted Intramolecular Charge Transfer State of Emerging Visible Light Photoswitches. *J. Photochem. Photobiol., A* **2019**, *371*, 336–340.
- (37) Curiac, C.; Hunt, L. A.; Sabuj, M. A.; Li, Q.; Baumann, A.; Cheema, H.; Zhang, Y.; Rai, N.; Hammer, N. I.; Delcamp, J. H. Probing Interfacial Halogen-Bonding Effects with Halogenated Organic Dyes and a Lewis Base-Decorated Transition Metal-Based Redox Shuttle at a Metal Oxide Interface in Dye-Sensitized Solar Cells. J. Phys. Chem. C 2021, 125 (32), 17647–17659.
- (38) Kohlrausch, R. Theorie des elektrischen Rückstandes in der Leidener Flasche. *Ann. Phys. Chem.* **1854**, *167* (2), 179–214.
- (39) Williams, G.; Watts, D. C. Non-Symmetrical Dielectric Relaxation Behaviour Arising from a Simple Empirical Decay Function. *Trans. Faraday Soc.* **1970**, *66*, 80.
- (40) Lindsey, C. P.; Patterson, G. D. Detailed Comparison of the Williams-Watts and Cole-Davidson Functions. *J. Chem. Phys.* **1980**, 73 (7), 3348–3357.
- (41) Lukichev, A. Physical Meaning of the Stretched Exponential Kohlrausch Function. *Phys. Lett. A* **2019**, 383 (24), 2983–2987.
- (42) Time-Domain Lifetime Measurements. In *Principles of Fluorescence Spectroscopy*; Lakowicz, J. R., Ed.; Springer US: Boston, MA, 2006; pp 97–155.